IOPscience iopscience.iop.org

Home Search Collections Journals About Contact us My IOPscience

Transient pauses of the bacterial flagellar motor at low load

This content has been downloaded from IOPscience. Please scroll down to see the full text.

2016 New J. Phys. 18 115002

(http://iopscience.iop.org/1367-2630/18/11/115002)

View the table of contents for this issue, or go to the journal homepage for more

Download details:

IP Address: 163.1.246.64
This content was downloaded on 24/11/2016 at 10:53

Please note that terms and conditions apply.

You may also be interested in:

Phosphatase localization in bacterial chemotaxis: divergent mechanisms, convergent principles
Christopher V Rao, John R Kirby and Adam P Arkin

Short time investigation of the neurospora kinesin step
Lorenzo Busoni, Aurélie Dupont, Clémentine Symonds et al.

The bacterial rotary motor
D F Blair

The hydrodynamics of swimming microorganisms
Eric Lauga and Thomas R Powers

Molecular energy transducers of the living cell. Proton ATP synthase: a rotating molecular motor
Yurii M Romanovsky and Alexander N Tikhonov

Advances in the microrheology of complex fluids
Thomas Andrew Waigh

Chemotaxis of Escherichia coli to L-serine
Rajitha R Vuppula, Mahesh S Tirumkudulu and K V Venkatesh

New Journal of Physics
The open access journal at the forefront of physics

Deutsche Physikalische Gesellschaft DPG
IOP Institute of Physics

Published in partnership with: Deutsche Physikalische Gesellschaft and the Institute of Physics

OPEN ACCESS

RECEIVED
30 June 2016

REVISED
22 October 2016

ACCEPTED FOR PUBLICATION
27 October 2016

PUBLISHED
23 November 2016

Original content from this work may be used under the terms of the Creative Commons Attribution 3.0 licence.

Any further distribution of this work must maintain attribution to the author(s) and the title of the work, journal citation and DOI.

PAPER

Transient pauses of the bacterial flagellar motor at low load

A L Nord[1,2,3], F Pedaci[2] and R M Berry[1]

[1] Department of Physics, University of Oxford, Parks Road, Oxford OX1 3PJ, UK
[2] Single Molecule Biophysics Department, Centre de Biochimie Stucturale, CNRS UMR 5048 UM INSERM U 1054, 29 Rue de Navacelles, 34090 Montpellier, France
[3] Author to whom any correspondence should be addressed.

E-mail: ashley.nord@cbs.cnrs.fr, francesco.pedaci@cbs.cnrs.fr and richard.berry@physics.ox.ac.uk

Keywords: *Escherichia coli*, bacterial flagellar motor, molecular motor, biophysics, darkfield microscopy

Supplementary material for this article is available online

Abstract

The bacterial flagellar motor (BFM) is the molecular machine responsible for the swimming and chemotaxis of many species of motile bacteria. The BFM is bidirectional, and changes in the rotation direction of the motor are essential for chemotaxis. It has previously been observed that many species of bacteria also demonstrate brief pauses in rotation, though the underlying cause of such events remains poorly understood. We examine the rotation of *Escherichia coli* under low mechanical load with high spatial and temporal resolution. We observe and characterize transient pauses in rotation in a strain which lacks a functional chemosensory network, showing that such events are a phenomenon separate from a change in rotational direction. Rotating at low load, the BFM of *E. coli* exhibits about 10 pauses s^{-1}, lasting on average 5 ms, during which time the rotor diffuses with net forwards rotation. Replacing the wild type stators with Na^+ chimera stators has no substantial effect on the pausing. We discuss possible causes of such events, which are likely a product of a transient change in either the stator complex or the rotor.

1. Introduction

The bacterial flagellar motor (BFM) is a membrane embedded protein complex that controls the motility and chemotaxis of many species of bacteria. The BFM couples energy from the ion motive force (IMF) into rotation of the flagella that propel the cell. The mechanochemical energy coupling is performed by stator protein complexes. The translocation of ions through a channel in the stator likely causes a conformational change in the stator which applies torque to the rotor and rotates the flagellar filament. In many species, the BFM switches direction stochastically, at a rate which is controlled by the chemotactic signaling system, allowing the cell to swim up a chemical gradient. The rotation speed of the BFM is known to be dependent upon IMF [1, 2], temperature [3], external load [4, 5], and the number of engaged stator protein units [6]. When these variables are held constant, rotation of the BFM is characterized by relatively constant absolute speed.

However, upon close examination, the BFM exhibits transient pauses in its otherwise steady rotation. Such pauses were first observed in 1974 [7, 8], and have since been observed in various species including *E. coli* [8–11], *Salmonella* [10], *Rhodobacter sphaeroides* [12], *Salmonella* Typhimurium [7, 10, 13], *Halobacterium halobium* [14], and *Rhizobium militobi* [15]. Chemical attractants and repellents decrease and increase, respectively, the fraction of time the motor spends in a paused state. While it was initially observed that motors of mutants which lack a large portion of the chemosensory networks do not pause [10], pauses have since been observed in strains lacking CheY, the chemotactic response regulator [9], though theses experiments were performed in a strain containing both functional and non-functional stators. While it was shown that pausing is not the result of a specific chemotactic signal distinct from that for reversal, and thus likely an intrinsic property of the motor [16], the nature of pauses in the BFM is still unknown. It has been proposed that they may be a product of incomplete reversals [16, 17], transient stator detachment [9], or something yet undiscovered. As it has been posited that they may induce tumbling of the bacterial cell, even in the absences of clockwise (CW) rotation [10], they may

© 2016 IOP Publishing Ltd and Deutsche Physikalische Gesellschaft

Table 1. List of strains used in this study.

Strain	Background	Plasmid	Genome
MTB22	YS34	*motAmotB* arabinose-inducible Amp ^{R}	Δ motAmotB ΔCheY Δ pilA Δ FilC Avi-Tag FlgE
YS1243	YS34	*pomApotB* IPTG-inducible Cm ^{R}	ΔmotAmotB ΔCheY Δ pilA Δ FilC

play a significant and unexamined role in bacterial chemotaxis. There is also evidence that intermittent pauses of the BFM may inhibit chi bacteriophage adsorption [11].

Though transient pauses lasting on the order of tens to hundreds of milliseconds seem to be an inherent feature of the BFM in many species, it was recently reported that the BFM sometimes toggles between maximum and zero speed on a timescale of ms [9]. Here we examine and characterize for the first time these fast transient pauses of the BFM with high angular and time resolution. Using backscattering dark field microscopy [18], we monitored the rotation of 100 nm gold nanoparticles attached to the hook of the BFM of a non-switching strain of *E. coli* with a resolution of ∼1.5° and ∼10 μs. We also performed these experiments for motors driven by Na^+ chimera stators [19]. The small load employed here reduces the relaxation time due to the elastic nature of the hook, which filters the readout of measurements performed with higher loads. Also, due to stator mechanosensing [5], only one or few stators should be active under such load, decreasing the complexity of the experimental interpretation. We resolve pauses in rotation and characterize the motion of the rotor during these events, and we discuss the potential biological causes and implications.

2. Materials and methods

2.1. Bacteria and culture

Two *E. coli* strains were used in this study, as detailed in table 1. Cells were grown from frozen aliquots (0.1 ml, grown overnight in LB medium and stored at −80 °C with glycerol, 25%v/v) in 5 ml of T-broth (1% Bacto tryptone (Difco), 0.5% NaCl) at 30 °C for 5.5 hrs. Cells were grown with appropriate antibiotics (ampicillin, 50 μg ml^{-1}, chloramphenicol 25 μg ml^{-1}) and inducers (arabinose, 20 μM, IPTG, 20 μM).

2.2. Speed measurements

Cells were immobilized on poly-L-lysine coated glass coverslips in custom-made flow chambers. Anti-rabbit IgG or streptavidin modified gold particles of 100 nm diameter (BBInternational) were attached to the hook via anti-FlgE antibody as described previously [9] for the Na^+ chimera stator experiments, or via the endogenously biotinylated AviTag sequence on the hook protein for the wildtype (WT) stator experiments [20], respectively. Experiments were performed in motility buffer (10 mM potassium phosphate, 0.1 mM EDTA, 85 mM potassium chloride, pH 7.0) at 23 °C. Beads were tracked using back-scattering darkfield microscopy [18] and a CMOS camera (Photron) at an acquisition rate of 109.5 kHz. A schematic of the assay is shown in figure 1(a).

2.3. Pause identification

All of the analysis was performed with custom Python and MATLAB programs. An ellipse was fit to the (x, y) position of the bead [21]. Based upon the ellipse fit, the ellipse was transformed to a circle and the angular position of the motor was determined. Speed was calculated as the change in angular position between each frame multiplied by the frame rate, then smoothed with a 0.5 ms (55 pt) window running mean filter. This signal was used to calculate the median speed of rotation. The raw angle trace was then low pass filtered with a cutoff frequency 15 times the median rotation speed (an average cutoff frequency of 1800 Hz), and subtracted from the original to yield the high frequency noise of the trace.

For each trace, small moving boxcar windows of angular rotation were examined individually. The window size was set to one fifth the median time for the BFM to complete one revolution. The slope and root-mean-square error (RMSE) of every window was determined via linear regression. Each window was then labeled as either spinning or stalled, based upon an analysis of simulated traces. The purpose of this step is to ensure that the trace has little enough noise to allow pausing and rotation to be adequately distinguished at the chosen timescale set by the window size, and it proceeded as follows. Two artificial traces were created for each

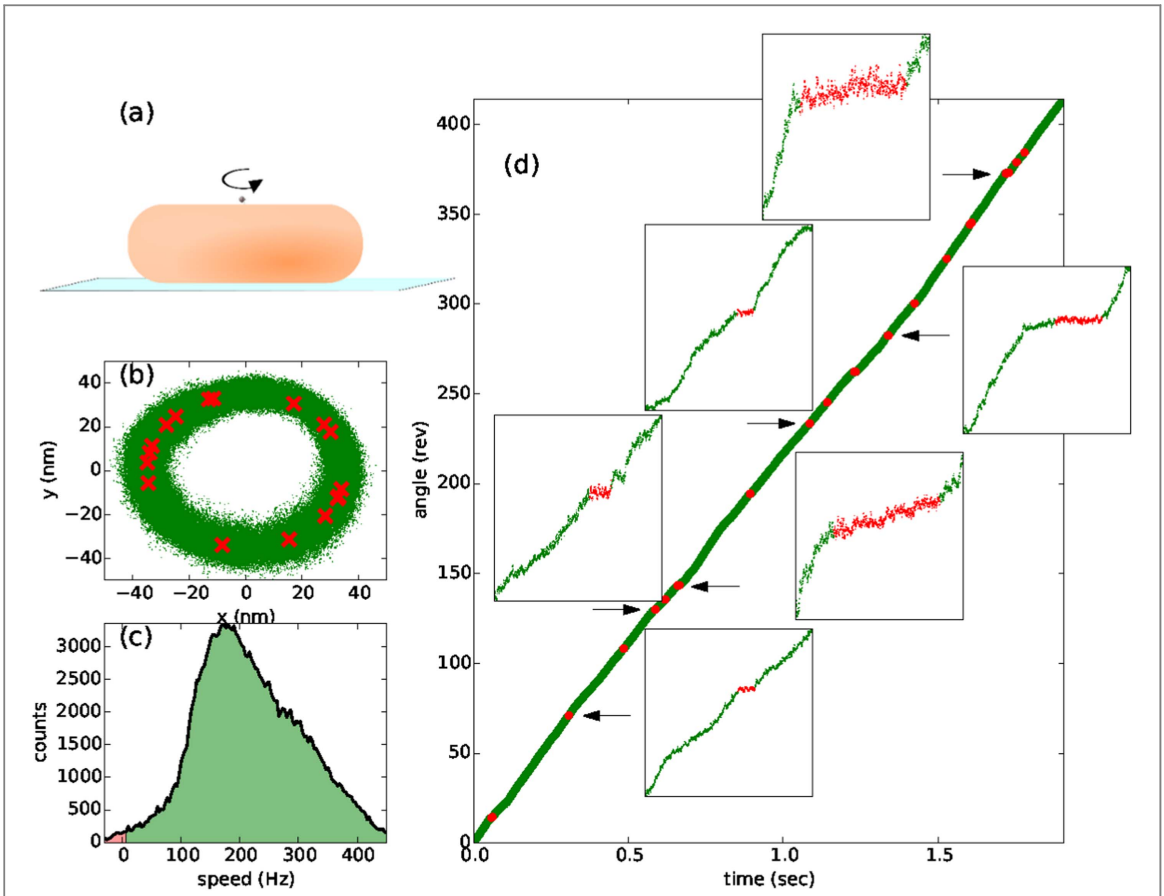

Figure 1. Experimental data. (a) Schematic of the assay, to scale. BFM rotation is observed via a 100 nm gold bead stuck to the hook of a BFM. (b)–(d) A typical trace of the WT motor, where green and red represent segments considered to be spinning and paused, respectively. (b) The bead's raw (x, y) position, with the start position of paused segments marked by a red x. (c) A histogram of all of the local slopes of the raw angle versus time trace, with green and red showing the cutoff that we applied between spinning and paused. (d) The bead's angular position. The insets show 10 ms portions at locations indicated by the arrows, each exhibiting one detected pause.

recording, one of constant rotation at the median speed of the recording, and the other stalled at zero speed. The high frequency noise obtained from the experimental trace was added to each artificial trace. The slope and RMSE of each window was determined for each of the artificial traces. Using a cutoff of 2.58 standard deviations (STD) (encompassing 99% of a Guassian distribution), it was first confirmed that the distribution of the simulated stalled and spinning slopes were well separated (that is, a speed 2.58 STDs greater than the mean stalled slope was less than a point 2.58 STDs less than the mean spinning slope). This was true for all experimental traces. If the slope and RMSE of any given window from the original recording was within the distribution of slopes and RMSEs of segments from the artificial stalled trace (again, using a threshold of 2.58 STDs), the center point of the window was classified as paused; if not, the window was classified as spinning. The moving boxcar approach meant that the beginning and end of a pause was identified as the center point of the first and last window to satisfy the pausing criteria. This analysis ensures that less than 1% of the windows will be incorrectly classified due to high frequency experimental noise. The choice of the window size matters: if too short it lacks statistical accuracy, and if too long it misses short paused events. Changing the window size by 10% caused a 3% variation in the average pause duration. In this way, the identification of real pauses reflected the experimental noise of each individual recording and was insensitive to rotation speed. This is a conservative definition of pauses which may miss events which occur on a time scale shorter than the window size (the average window size was 1.7 ms).

In order to further validate the above method of pause identification, additional simulated traces were created in the following manner. Kinetic Monte Carlo (KMC) methods (Gillespie algorithm) were used to model a Poisson stepper which takes 26 steps per revolution [22] with each mechanical step a composite of three rate-limiting chemical processes with identical rate. While the number and rate of chemical processes within the mechanochemical cycle of the staor is unknown, we have chosen three processes to represent ion binding from the periplasm, ion translocation, and ion unbinding into the cytoplasm. This makes for 78 processes per revolution, though it is possible that not all these processes are rate-limiting. Pauses of varying duration were introduced at regular intervals. The kinetic rate of stator chemical processes was set such that the rotation speed

of the simulated traces matched those of the real data, as did the amplitude and spectrum of the high frequency noise which was added to the traces. Our KMC simulations generate a statistically correct time evolution of the stochastic stepping rotation of the BFM with the above mentioned states and transition rates between states, under the assumption that the sequence of states is Markovian and Poisson distributed. When the pause identification algorithm was applied to these simulated traces, the false-positive identification rate was zero. The algorithm correctly identified all the pauses which were of the same duration or longer than the window size and recovered their duration with an accuracy of ~0.07 ms. An example of the algorithm applied to a simulated trace is shown in SI figure 1.

2.4. Mean displacements (MD) and mean square displacements (MSD) analysis

The displacement of the bead was calculated over integer numbers of video frames during each detected pause and each spinning episode. Our algorithm identified 365 (527) pauses in wildtype (chimeric) motors. These pauses contained a total of ~180 000 (~326 000) measurements of the displacement over a single frame (9.1 μs). We pooled displacement measurements over all pauses (and similarly for spinning episodes) in each type of motor to calculate the MD and the MSD as a function of elapsed time. The pauses contained a total of 403 (873) non-overlapping intervals of 2 ms in 98 (201) stalls, corresponding to standard errors of the MSD of 8% (13%) for this time interval under a Gaussian model. We chose 2 ms as a reasonable upper time limit for MD and MSD analysis—longer intervals are increasingly poorly sampled and correspondingly yield excessively noisy MDs and MSDs.

The theoretical value of the drag coefficient of the motor was calculated as the sum of the drag coefficient of the bead and rotor

$$\gamma = 8\pi\eta_b r_b^3 + 6\pi\eta_b r_b r_e^2 + 8\pi\eta_c r_{rot}^3, \quad (1)$$

where r_b and r_e are the bead radius and radius of eccentricity, η_b and η_c are the viscosities of the buffer and cytoplasm [23, 24], and r_{rot} is the radius of the rotor [25]. The diffusion coefficient of the system is

$$D = \frac{k_B T}{\gamma}, \quad (2)$$

where k_B is the Boltzmann constant and T is the temperature.

3. Results

3.1. Rotational measurements and pause identification

Gold nanoparticles of 100 nm diameter were stuck to the hook of the BFM. With an experimental resolution of ~1.5° and ~10 μs, these experiments represent the best spatial and time resolution of BFM rotation to date. More than 35 s of data from more than 15 cells were collected both for the WT and Na^+ chimera stator strains, yielding motor position over five orders of magnitude in time.

More than 200 pauses were detected and analyzed for each of the two strains. See figure 1 for example pauses in the WT motor. With the criteria as defined in materials and methods, pauses have been identified in a manner that considers the high frequency noise of the raw data and is insensitive to native motor speed, ensuring that identified pauses are not an artifact of experimental noise. Additionally, when the pause identification algorithm was applied to simulated traces of a Poisson stepper with noise matching experimental levels, no false pauses were found, and all real pauses larger than the window size were successfully identified. This indicates that the pauses which are observed in the experimental data are unlikely to be artifacts due to experimental noise, and can not be explained by the model of an incessantly rotating Poisson stepper. The spatial distribution of pauses was examined, and no obvious pattern was found (see SI figure 2). It thus seems unlikely that the pauses identified are due to interactions between the gold particles and the cell surface.

The statistics of the pauses in BFM rotation are shown in figure 2. The distribution of pause durations is reasonably well fit by a single exponential (solid line) for both the WT and Na^+ chimera motors. WT cells at low load spend 4.9 ± 6.2% of their time paused, with a pause frequency of 10.7 ± 7.2 pauses per second and an average pause duration of 4.6 ± 6.0 ms. Na-stator cells spend 10.8 ± 10.2% of their time paused, with a pause frequency of 16.1 ± 11.9 pauses per second and an average pause duration of 6.7 ± 13.7 ms (all values refer to mean ± STD calculated over all cells). The large cell to cell variability in pause duration and frequency is shown in figure 2(c). We also compared the distribution of pause durations to the distribution of dwell time durations from our simulated traces (shown in SI figure 3) in order to confirm that the former was unlikely to be a subpopulation of the later.

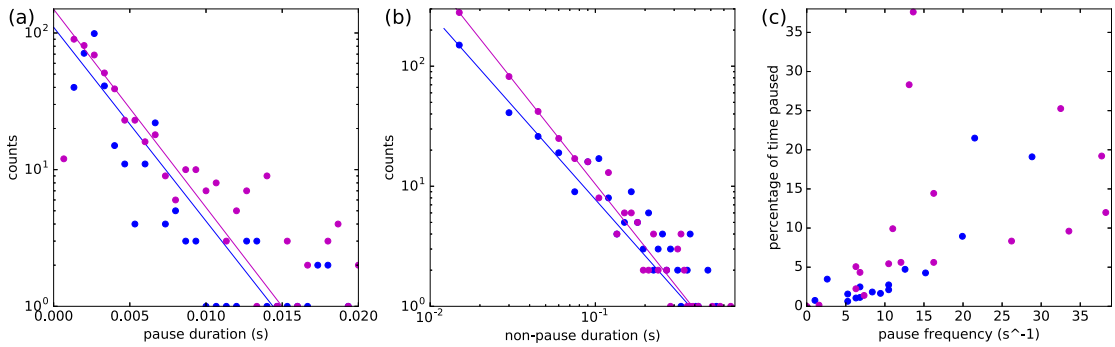

Figure 2. Characterization of the pauses in BFM rotation. Blue and magenta represent the WT and Na^+ chimera motor, respectively. (a) The distribution of pause duration is fit by a single exponential (solid line). (b) The distribution of non-paused duration. The solid line is the best fit of a power law. (c) The percentage of time the BFM spends in the paused state versus the frequency of pauses, where each point represents one motor.

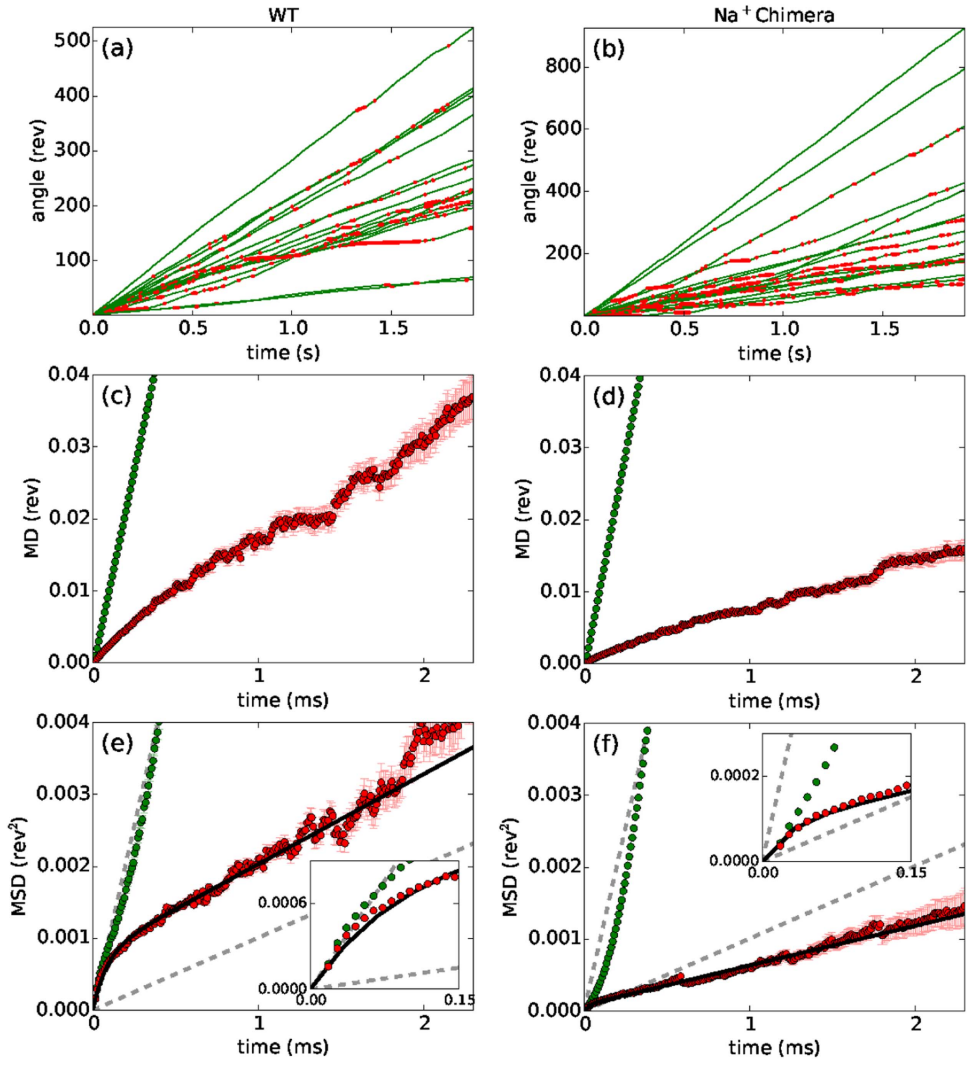

Figure 3. Short time scale displacement of the motor during spinning and paused segments. (a) and (b) angle versus time of the WT and Na^+ chimera motors, respectively, where green and red mark spinning and paused segments, respectively. (c) and (d) mean displacement (MD) as a function of time of the spinning (green) and stalled (red) segments shown in (a)–(b). Net mean forward movement is observed during the pauses. (e) and (f) mean squared displacement (MSD) as a function of time of the spinning (green) and stalled (red) segments shown in (a) and (b). The gray dashed lines represent a theoretical range of values of the MSD of a 100 nm bead on a motor under Brownian motion. The black line is the fit of the pause MSD data to the superposition of two diffusive processes, as discussed in section 3.2. In (c)–(f), in the wild-type (chimeric) motor, at 2 ms the MD or MSD is an average of 403 (873) windows from 98 (201) stalls. In all cases, error bars represent the standard error (SE); where not visible, the SE is smaller than the marker.

3.2. Displacement during pauses

Figures 3(a) and (b) show the angle versus time of all the recordings for the WT and Na^+ chimera motors, with their paused segments identified. Figures 3(c) and (d) show MD versus elapsed time for spinning (green) and paused (red) episodes. On average, the rotor demonstrates net forward motion during the pauses. Figures 3(e) and (f) show MSD versus elapsed time for spinning (green) and paused (red) episodes. Between ~0.1 ms and ~2 ms, MSD is quadratic for spinning episodes as expected for rotation at a constant speed, and linear for paused episodes, indicating free rotational diffusion on these timescales, with diffusion coefficients of 1.4 $rev^2\ s^{-1}$ and 0.6 $rev^2\ s^{-1}$ for WT and chimera respectively. Below ~0.1 ms, MSD curves for both spinning and stalled episodes are approximately linear, but with considerably larger slopes. Timescales longer than 2 ms are not sampled adequately due to the short lifetime of pauses. A single diffusion process is not sufficient to describe these MSD curves; as discussed further below, we hypothesize that they can be understood as the superposition of two diffusive processes: one fast and confined, giving a steep gradient at short times and a plateau at long times ($MSD_1 = A(1 - e^{t/t_0})$); the other slow and unconfined, adding a second term $MSD_2 = Bt$, where t is elapsed time and $A = \langle\theta_1^2\rangle$, $t_0 = \langle\theta_1^2\rangle/D_1$ and $B = 2D_2$ are constants, with θ_i and D_i the angular displacements and diffusion coefficients of each diffusive process. The relation between t_0, $\langle\theta_1^2\rangle$ and D_1 may be simply derived from the Einstein relation $D_1\gamma_1 = k_B T$, the principle of equipartition of energy which gives $k_B T = \kappa_1\langle\theta_1^2\rangle$ and the corner frequency $f_{c,1} = 1/t_0 = \kappa_1/\gamma_1$, where κ_1 and γ_1 are the stiffness and viscous drag coefficients respectively of the fast process, k_B is the Boltzmann constant and T is temperature. The relation between B and D_2 follows from the identity $\langle\theta_2^2\rangle = 2D_2 t$ for free diffusion in one-dimension. Fitting MSD curves as the sum of $MSD_1 + MSD_2$ (figures 3(c) and (d), black line) gives ($\langle\theta_1^2\rangle$, D_1, D_2) = (7.8×10^{-4} rev^2, 9.2 $rev^2\ s^{-1}$, 0.6 $rev^2\ s^{-1}$) and (8.4×10^{-4} rev^2, 3.2 $rev^2\ s^{-1}$, 0.3 $rev^2\ s^{-1}$) for WT and chimera respectively. The gray dashed lines show theoretical MSDs for free rotational diffusion of a 100 nm bead attached to the hook of a BFM, as detailed in materials and methods. The large range is due to different measured values of the cytoplasm viscosity, from 50 to 700 times that of water [23, 24]. The diffusion coefficients of the fast and slow processes are similar to the upper and lower theoretical estimates respectively.

3.3. Angular position of pauses

The angular positions of the motor stalls were examined for pattern or periodicity, testing whether an underlying molecular organization could be revealed. Examination of the cumulative pairwise distribution function (PDF) and power spectral density of the angular position of all the pauses in all the motors (shown in SI figure 4) revealed no global periodicity. An examination of the PDF of individual pauses showed that while about 90% of pauses show no periodicity, about 10% of pauses show one or multiple peaks in the PDF, consistent with one or multiple steps of the rotor during the pause. Examples of such pauses are shown in SI figure 4.

4. Discussion

Pausing of the BFM has been observed since the very first rotation experiments. Since the first observation that the number and duration of pauses increased with the addition of repellents and decreased with the addition of attractants [10], it was further clarified that the frequency of pausing correlates with the frequency of switching, with no separate chemotactic signal found for pausing. This suggested that pausing is the result of futile (or incomplete) switching events [16]. Furthermore, it was observed that a strain that lacks chemotaxis machinery does not pause (at high load) [10]. Given the direct detection of incomplete switching events, explained by the conformational spread model [17], it seems plausible that previously observed pauses of BFM rotation can be ascribed to incomplete switching events. Our measurements have increased the time resolution by a factor of at least 2000 over early observations of pausing [10, 11, 16] and by a factor of ~100 over the more recent work on conformational spread [17]. Using a similar gold nanoparticle labelling of the motor to ours, but ~35 times slower sampling, it was recently observed that a ΔCheY mutant exhibits transient toggles between maximum speed and zero speed at low load [9]. Motors of strains lacking CheY do not switch direction [26]. Thus, in the absence of CheY , as in our measurements, transient pauses can not be explained by incomplete switching events. Therefore these pauses may be a separate phenomenon from pauses that have previously been seen in BFM rotation, and the nature of such events is thus far unknown.

We find that, at low load, wild type *E. coli* spends about 5% of its time in the transiently paused state, but that the pauses are brief: on average 5 ms. Using a strain where the wild type stators have been replaced by Na^+ chimera stators has no significant impact on the frequency or duration of pauses. In both cases, the distribution of pause times is exponential, suggesting that it is the product of a single stochastic process. Multiple models of the BFM predict either an exponential or stretched exponential distribution of dwell times of the motor [27, 28], where dwell times are defined as the period in between mechanical steps, presenting the possibility that the measured pauses are simply the tail of the dwell time distribution. In SI figure 3 we have compared the predicted

dwell time distribution of a Poisson stepper (as described in materials and methods) to our measured pause distribution. The difference between the distributions of rotation speeds shown in figure 1(c) and SI figure 1(b) suggests that the pauses are in fact a separate phenomenon, and that our criteria for identifying pauses are conservative; the slow tail of the measured distribution may indicate pause-like events that are too short for our algorithm to detect.

The existence of brief transient pauses in BFM rotation could arise under a number of scenarios, an effect of a transient change in either the stator or the rotor. Pausing due to the stator could occur either at the interface with the C-ring or by disengagement from the cell wall. The former would allow the possibility of periodic interaction potentials, possibly inherent to the mechanochemical cycle of the stator as observed in other molecular motors [29, 30]. Either type of stator pause could be the same process as IMF- or load-dependent stator disengagement, possibly linked to transient fluctuations in local IMF or load. One possibility for pausing due to the rotor is transient directional switching of one or more units in the C-ring, hypothesized to correspond to different structures of the C-ring protein FliG [31, 32], as required in the conformational-spread model of the flagellar switch [17, 33]. The conformational spread model estimates that a single stator unit has an 8% chance of encountering a FliG subunit which is in the state that supports CW rotation, even in the absence of CheY [34]. This is close to the fraction of detected backwards steps in [22] and of detected pauses in this study. A motor with a single stator unit would get stuck at the junction between CW and counterclockwise domains of FliG. The transient formation and diffusion of such junctions [17] and their interaction with fully functional single stator units could explain the existence of pauses and the rotational behavior during pauses. Alternatively, as rotor components such as FliM and FliN are known to turnover [35–37], it is possible that pauses occur when a single stator unit encounters a transient 'hole' in the rotor which it can not pass, though we note that FliG is currently not believed to turnover [37]. Finally, for motors driven by multiple units, the above scenarios remain valid though more complex, with the possibility of a tug-of-war between units, or the inactivity of one unit jamming or hindering the activity of others. We suspect that at higher load, and thus higher stator number [4, 5], the frequency of motor pauses may decrease, as transient events of a single stator unit become masked by the functioning of other stator units, or because the stator units may be more stable at high load. However, a larger external load increases the relaxation time of the bead, decreasing the chances of resolving such brief events.

Our unprecedented temporal resolution of 10 μs combined with a short relaxation time of the bead on the hook allows characterization of the fluctuations in motor angle on sub-millisecond timescales. Analysis of the dependence of MSD upon elapsed time showed two diffusive processes during pauses, one fast and constrained, the other slower and unconstrained. Perhaps the simplest explanation of the fast diffusive process is Brownian motion of the bead on the hook relative to the rotor, due to both torsional and bending compliance of the hook. Hook compliance is expected to show the observed signature of constrained Brownian motion in the bead position, which would add to the signal due to rotation of the rotor. While nothing is known about the bending compliance of the hook, the torsional compliance has been measured [20, 38, 39] and allows an estimate of the relaxation time of a tethered 100 nm gold bead as 5–32 μs. From the fits in figures 3(c) and (d), the characteristic relaxation time for the fast diffusive process ($t_0 = \langle\theta_1^2\rangle/D_1$) is 85 and 26 μs for WT and chimera motors, respectively. This is consistent with the above estimate for torsional Brownian compliance of the hook: while the hook torsional compliance in our experiment is expected to be lower than the previously measured value, because the bead is presumably attached part-way along the hook, this is probably offset by the effects of bending compliance, which are undetected in the tethered cell assay in which hook compliance was originally measured. If the fast process is indeed due to hook compliance, the three fold difference between WT and chimera relaxation times is most likely explained by the different tethering methods used. This would indicate that antibody tethering stiffens the hook three times more than biotin–avidin.

The slow and unconstrained diffusive process is also faster in WT than chimera, by a factor of two, indicating that this process is at least partially dependent upon the stator. Net forward rotation during pauses revealed by MD analysis indicates furthermore that free energy is coupled to this process. The simplest explanation is that stators are still at least partially engaged, and partially or intermittently functional, during pauses. We offer two models for this, with the possibility that both may be required to explain the observed heterogeneity in stepping behavior during pauses. The first model would be that stators fully disengage (and diffuse freely), intermittently but too fast to resolve, during pauses. Net rotation would occur between disengagements, and dependence upon stator type would be via the timing and nature of transient engagements. The second model postulates a static periodic interaction potential between a non-functioning stator and the rotor [22, 40–42]. Hopping diffusion in this potential would give the observed linear dependence of MSD upon elapsed time, with a diffusion coefficient determined by the periodicity and amplitude of the potential [43]. Net forward rotation would be explained either as above, by intermittent functioning of the stator, or by functioning stator units driving unidirectional stepping in a periodic interaction potential of non-functioning stator units. This model would explain in particular the stepping rotation observed in ~10% of pauses (SI figure 4). The step size in these pauses is often consistent with the 26-fold periodicity observed previously in partially de-energized chimera motors [22], which

may indicate that the same interaction potential is responsible (SI figure 4). Extrapolation of the data of figures 3(c) and (d) gives a mean displacement of about 1/15 (WT) or 1/30 (chimera) of a revolution in the mean pause duration of 5 ms. Similarly, extrapolation of figures 3(e)–(f) gives root-mean-square displacements of 1/12 or 1/18 rev in 5 ms for the slow diffusive process. These indicate that if the step-size is 1/26 rev, the number of steps taken in each pause is small. In both WT and Na^+ chimera motors, the localization of stator units around the rotor is IMF dependent [42, 44–46]. It was previously observed that, upon IMF depletion, units do not immediately diffuse away, but remain localized with the motor for about 30 s, during which time the rotation of the rotor is constrained [42]. This constraint may be the same as the periodic interaction potential proposed in the second model above. Finally, we note here the possibility that we have overestimated the relaxation times for hook compliance, which may be much shorter than that of the observed fast process. If this were true, the best explanation for the fast process would be diffusion within individual wells of a periodic rotor–stator potential.

5. Conclusion

This study represents the first characterization of sub-millisecond transient pauses in the BFM at low load, with high angular and temporal resolution. Given the current model of switching in the BFM, we expect that some pauses of BFM rotation which have been observed in strains with functional chemosensory networks can be explained by incomplete switching of the switch complex. However, as characterized here, the BFM in absence of CheY also exhibits transient pauses of short duration which are not able to be explained in this way. These brief transient pauses of motor rotation could be due to transient deactivation or detachment of the stator complex, transient thermal flipping of a FliG subunit, or a transient 'hole' in the rotor protein ring. We expect that further explorations into the nature of these events will provide information about the nature of the mechanochemical cycle and the mechanosensitity of the stator complex.

Acknowledgments

We thank M T Brown for help constructing bacterial strains. RMB and ALN acknowledge funding from the Biotechnology and Biological Sciences Research Council, grant number BB/H01991X/1. FP and ALN acknowledge funding from the European Research Council under the European Union's Seventh Framework Programme (FP/2007-2013)/ERC Grant Agreement n. 306475. ALN acknowledges funding from the Rhodes Trust.

References

[1] Fung D C and Berg H C 1995 Powering the flagellar motor of escherichia coli with an external voltage source *Nature* **375** 809–12
[2] Gabel C V and Berg H C 2003 The speed of the flagellar rotary motor of escherichia coli varies linearly with protonmotive force *Proc. Natl Acad. Sci. USA* **100** 8748–51
[3] Berg H C and Turner L 1993 Torque generated by the flagellar motor of escherichia coli *Biophy. J.* **65** 2201–16
[4] Tipping M J, Delalez N J, Lim R, Berry R M and Armitage J P 2013 Load-dependent assembly of the bacterial flagellar motor *mBio* **4** e00551-13
[5] Lele P P, Hosu B G and Berg H C 2013 Dynamics of mechanosensing in the bacterial flagellar motor *Proc. Natl Acad. Sci.* **110** 11839–44
[6] Ryu W S, Berry R M and Berg H C 2000 Torque-generating units of the flagellar motor of escherichia coli have a high duty ratio *Nature* **403** 444–7
[7] Macnab R and Koshland D E 1974 Bacterial motility and chemotaxis: light-induced tumbling response and visualization of individual flagella *J. Mol. Biol.* **84** 399–406
[8] Silverman M and Simon M 1974 Flagellar rotation and the mechanism of bacterial motility *Nature* **249** 73–4
[9] Yuan J and Berg H C 2008 Resurrection of the flagellar rotary motor near zero load *Proc. Natl Acad. Sci. USA* **105** 1182–5
[10] Lapidus I R, Welch M and Eisenbach M 1988 Pausing of flagellar rotation is a component of bacterial motility and chemotaxis *J. Bacteriol.* **170** 3627–32
[11] Ravid S and Eisenbach M 1983 Correlation between bacteriophage chi adsorption and mode of flagellar rotation of escherichia coli chemotaxis mutants *J. Bacteriol.* **154** 604–11
[12] Armitage J P and Macnab R M 1987 Unidirectional, intermittent rotation of the flagellum of rhodobacter sphaeroides *J. Bacteriol.* **169** 514–8
[13] Kudo S, Magariyama Y and Aizawa S 1990 Abrupt changes in flagellar rotation observed by laser dark-field microscopy *Nature* **346** 677–80
[14] Marwan W, Alam M and Oesterhelt D 1991 Rotation and switching of the flagellar motor assembly in halobacterium halobium *J. Bacteriol.* **173** 1971–7
[15] Götz R and Schmitt R 1987 Rhizobium meliloti swims by unidirectional, intermittent rotation of right-handed flagellar helices *J. Bacteriol.* **169** 3146–50
[16] Eisenbach M, Wolf A, Welch M, Caplan S R, Lapidus I R, Macnab R M, Aloni H and Asher O 1990 Pausing, switching and speed fluctuation of the bacterial flagellar motor and their relation to motility and chemotaxis *J. Mol. Biol.* **211** 551–63
[17] Bai F, Branch R W, Nicolau D V, Pilizota T, Steel B C, Maini P K and Berry R M 2010 Conformational spread as a mechanism for cooperativity in the bacterial flagellar switch *Science* **327** 685–9

[18] Sowa Y, Steel B C and Berry R M 2010 A simple backscattering microscope for fast tracking of biological molecules *Rev. Sci. Instrum.* **81** 113704
[19] Asai Y, Yakushi T, Kawagishi I and Homma M 2003 Ion-coupling determinants of Na+-driven and H+-driven flagellar motors *J. Mol. Biol.* **327** 453–63
[20] Brown M T, Steel B C, Silvestrin C, Wilkinson D A, Delalez N J, Lumb C N, Obara B, Armitage J P and Berry R M 2012 Flagellar hook flexibility is essential for bundle formation in swimming escherichia coli cells *J. Bacteriol.* **194** 3495–501
[21] Fitzgibbon A, Pilu M and Fisher R B 1999 Direct least square fitting of ellipses *IEEE Trans. Pattern Anal. Mach. Intell.* **21** 476–80
[22] Sowa Y, Rowe A D, Leake M C, Yakushi T, Homma M, Ishijima A and Berry R M 2005 Direct observation of steps in rotation of the bacterial flagellar motor *Nature* **437** 916–9
[23] Kalwarczyk T, Tabaka M and Holyst R 2012 Biologistics-diffusion coefficients for complete proteome of escherichia coli *Bioinformatics* **28** 2971–8
[24] Kuimova M K, Botchway S W, Parker A W, Balaz M, Collins H A, Anderson H L, Suhling K and Ogilby P R 2009 Imaging intracellular viscosity of a single cell during photoinduced cell death *Nat. Chem.* **1** 69–73
[25] DePamphilis M L and Adler J 1971 Fine structure and isolation of the hook-basal body complex of flagella fromescherichia coliandbacillus subtilis *J. Bacteriol.* **105** 384–95
[26] Wolfe A J, Conley M P, Kramer T J and Berg H C 1987 Reconstitution of signaling in bacterial chemotaxis *J. Bacteriol.* **169** 1878–85
[27] Mora T, Yu H, Sowa Y and Wingreen N S 2009 Steps in the bacterial flagellar motor *PLoS Comput. Biol.* **5** 1000540
[28] Meacci G and Tu Y 2009 Dynamics of the bacterial flagellar motor with multiple stators *Proc. Natl Acad. Sci. USA* **106** 3746–51
[29] Dangkulwanich M, Ishibashi T, Liu S, Kireeva M L, Lubkowska L, Kashlev M and Bustamante C J 2013 Complete dissection of transcription elongation reveals slow translocation of RNA polymerase II in a linear ratchet mechanism *eLife* **2** e00971
[30] Dulin D, Vilfan I D, Berghuis B A, Hage S, Bamford D H, Poranen M M, Depken M and Dekker N H 2015 Elongation-competent pauses govern the fidelity of a viral RNA-dependent RNA polymerase *Cell Rep.* **10** 983–92
[31] Lee L K, Ginsburg M A, Crovace C, Donohoe M and Stock D 2010 Structure of the torque ring of the flagellar motor and the molecular basis for rotational switching *Nature* **466** 996–1000
[32] Nakamura S, Kami-ike N, Yokota J I P, Minamino T and Namba K 2010 Evidence for symmetry in the elementary process of bidirectional torque generation by the bacterial flagellar motor *Proc. Natl Acad. Sci.* **107** 17616–20
[33] Duke T A, Le Novere N and Bray D 2001 Conformational spread in a ring of proteins: a stochastic approach to allostery *J. Mol. Biol* **308** 541–53
[34] Mandadapu K K, Nirody J A, Berry R M and Oster G 2015 Mechanics of torque generation in the bacterial flagellar motor *Proc. Natl Acad. Sci. USA* **112** E4381-9
[35] Delalez N J, Berry R M and Armitage J P 2014 Stoichiometry and turnover of the bacterial flagellar switch protein flin *mBio* **5** e01216-14
[36] Delalez N J, Wadhams G H, Rosser G, Xue Q, Brown M T, Dobbie I M, Berry R M, Leake M C and Armitage J P 2010 Signal-dependent turnover of the bacterial flagellar switch protein flim *Proc. Natl Acad. Sci. USA* **107** 11347–51
[37] Fukuoka H, Inoue Y, Terasawa S, Takahashi H and Ishijima A 2010 Exchange of rotor components in functioning bacterial flagellar motor *Biochem. Biophys. Res. Commun.* **394** 130–5
[38] Block S M, Blair D F and Berg H C 1991 Compliance of bacterial polyhooks measured with optical tweezers *Cytometry* **12** 492–6
[39] Block S M, Blair D F and Berg H C 1989 Compliance of bacterial flagella measured with optical tweezers *Nature* **338** 514–8
[40] Mora T, Yu H, Sowa Y and Wingreen N S 2009 Steps in the bacterial flagellar motor *PLoS Comput. Biol.* **5** 1000540
[41] Pilizota T, Brown M T, Leake M C, Branch R W, Berry R M and Armitage J P 2009 A molecular brake, not a clutch, stops the rhodobacter sphaeroides flagellar motor *Proc. Natl Acad. Sci. USA* **106** 11582–7
[42] Sowa Y, Homma M, Ishijima A and Berry R M 2014 Hybrid-fuel bacterial flagellar motors in escherichia coli *Proc. Natl Acad. Sci. USA* **111** 3436–41
[43] Dean D S and Oshanin G 2014 Approach to asymptotically diffusive behavior for brownian particles in periodic potentials: extracting information from transients *Phys. Rev.* E **90** 062114
[44] Tipping M J, Steel B C, Delalez N J, Berry R M and Armitage J P 2013 Quantification of flagellar motor stator dynamics through in vivo proton-motive force control *Mol. Microbiol.* **87** 338–47
[45] Fukuoka H, Wada T, Kojima S, Ishijima A and Homma M 2009 Sodium-dependent dynamic assembly of membrane complexes in sodium-driven flagellar motors *Mol. Microbiol.* **71** 825–35
[46] Sowa Y and Berry R M 2008 Bacterial flagellar motor *Q. Rev. Biophys.* **41** 103–32